IOPscience iopscience.iop.org

Home Search Collections Journals About Contact us My IOPscience

A piezoelectric device for impact energy harvesting

This article has been downloaded from IOPscience. Please scroll down to see the full text article.

2011 Smart Mater. Struct. 20 105008

(http://iopscience.iop.org/0964-1726/20/10/105008)

View the table of contents for this issue, or go to the journal homepage for more

Download details:
IP Address: 193.48.219.28
The article was downloaded on 02/09/2011 at 07:38

Please note that terms and conditions apply.

Smart Mater. Struct. **20** (2011) 105008 (12pp) doi:10.1088/0964-1726/20/10/105008

A piezoelectric device for impact energy harvesting

E Jacquelin[1,3], S Adhikari[2] and M I Friswell[2]

[1] Université Lyon 1, IFSTTAR, UMR_T9406, LBMC, Université de Lyon, Lyon, F-69003, France
[2] College of Engineering, Swansea University, Singleton Park, Swansea SA2 8PP, UK

E-mail: eric.jacquelin@univ-lyon1.fr, S.Adhikari@swansea.ac.uk and M.I.Friswell@swansea.ac.uk

Received 4 April 2011, in final form 30 June 2011
Published 31 August 2011
Online at stacks.iop.org/SMS/20/105008

Abstract
This paper studies a piezoelectric impact energy harvesting device consisting of two piezoelectric beams and a seismic mass. The aim of this work is to find the influence of several mechanical design parameters on the output power of such a harvester so as to optimize its performance; the electrical design parameters were not studied. To account for the dynamics of the beams, a model including the mechanical and piezoelectric properties of the system is proposed. The impacts involved in the energy harvesting process are described through a Hertzian contact law that requires a time domain simulation to solve the nonlinear equations. A transient regime and a steady-state regime have been identified and the performance of the device is characterized by the steady-state mean electrical power and the transient electrical power. The time simulations have been used to study the influence of various mechanical design parameters (seismic mass, beam length, gap, gliding length, impact location) on the performance of the system. It has been shown that the impact location is an important parameter and may be optimized only through simulation. The models and the simulation technique used in this work are general and may be used to assess any other impact energy harvesting device.

1. Introduction

Piezoelectric systems have many applications including the development of sensors, actuation, and health monitoring. In this paper piezoelectric cantilevered beams are used to harvest energy: the ambient vibration energy is converted to electrical energy by the piezoelectric properties. The ambient vibration energy produces a base excitation that may be harmonic [1], broadband random [2], or a set of impulses. Improvements to the device may increase the deformation of the piezoelectric material and thus increase the generated current: for example, a seismic mass may be placed at the tip of the cantilevered beam [1, 3], or additional impact pulses [3–5] may be used leading to impact energy harvesting. The latter is the focus of this paper.

Piezoelectric cantilevered harvesters have been widely studied. Smits *et al* [6] derived the constituent equations for bimorphs. Wang *et al* [7] and Ballas *et al* [8] extended this work to all kinds of piezoelectric systems. However, these analyses are based on continuous beam theory and do not lead to a simple model with a finite number of degrees of freedom (dof) that is able to study the dynamic response of piezoelectric cantilevered beams. For design purposes, single-dof systems have been developed [9]. Erturk *et al* [10] highlighted the fact that these models must be used carefully and may fail to represent the piezoelectric coupling. Some authors [1, 9, 11] have proposed a modal approach to deal with the distributed parameter model of a piezoelectric system. Similarly, a Rayleigh–Ritz approach was used by several authors [9, 12]. The finite element method [13, 14] has also been considered to model a piezoelectric harvester. The goal of the Rayleigh–Ritz approach and the modal model is to obtain closed-form expressions of the piezoelectric beam response. However, for impact energy harvesting only numerical responses may be obtained even though some quantities may be estimated by simplifying the impact force [4, 15, 16]

The model used in this paper uses the Rayleigh–Ritz approach. An appropriate choice of the Rayleigh–Ritz functions/vectors leads to a multi-dof system that may be

[3] On a 6-month academic sabbatical leave at Swansea University in 2011.

 © 2011 IOP Publishing Ltd Printed in the UK & the USA

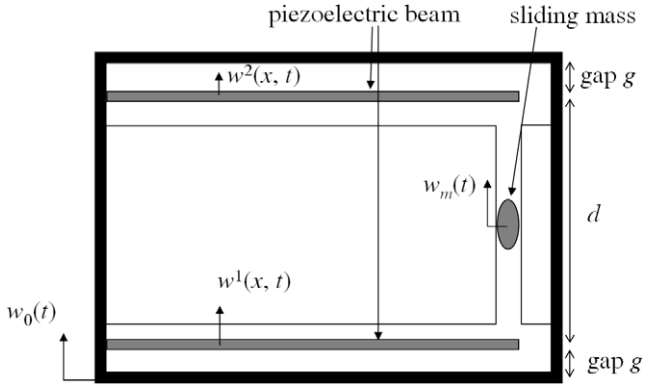

Figure 1. Schematic of the piezoelectric harvester.

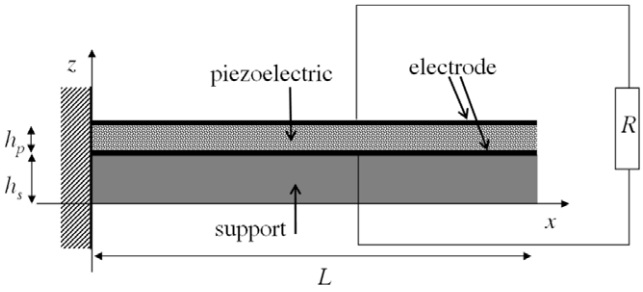

Figure 2. Schematic of the piezoelectric unimorph.

considered to be a set of spring–mass systems. This model [17–19] is referred to as an anti-oscillator (AO) model and has proved efficient to model impacted structures [20]. Here it will be used to model impacted piezoelectric beams.

This paper provides models and techniques that enable the optimization of the mechanical design parameters of an impact energy harvesting device. This is illustrated through an existing impact energy harvester developed by Renaud *et al* [3, 4]. This paper is organized as follows. The piezoelectric impact energy harvesting device studied in this paper is described first. Then, the AO-model is presented briefly. The equations that govern the device response are established and then discretized. Finally a sensitivity analysis is performed to determine the influence of some mechanical design parameters on the performance of the piezoelectric device.

2. Description of the system

The system studied was described by Renaud *et al* [3, 4] and consists of a box that encloses two identical cantilevered piezoelectric unimorphs impacted by a sliding mass at the tip of the beam (see figure 1). d is the distance between the beams. Each beam shown in figure 2 has its tip displacement limited by a stop (gap g) between the beam and the box internal wall. The z-axis is in the beam thickness direction with origin at the bottom of the beam (free surface of the support). Each unimorph is characterized by

- the support thickness (h_s),
- the piezoelectric thickness (h_p),
- the beam thickness ($h = h_s + h_p$),
- the beam width (W),
- the mass density of the constituents (piezoelectric: ρ_p; support: ρ_s),
- the mechanical properties:
  - * support Young's modulus (Y_s),
  - * piezoelectric Young's modulus at a constant electric field ($\tilde{c}_{11}^E$),
  - * piezoelectric compliance at a constant electric field ($s_{11}^E = 1/\tilde{c}_{11}^E$),
- the piezoelectric constants ($\tilde{e}_{31}$, $d_{31} = \tilde{e}_{31} \times s_{11}^E$),
- the permittivity component at constant strain with the plane stress assumption ($\tilde{\epsilon}_{33}^S$),
- the permittivity component at constant stress ($\tilde{\epsilon}_{33}^T = \tilde{\epsilon}_{33}^S + d_{31}^2/s_{11}^E$).

The rigid box has a translational movement $w_0(t)$ which is the base excitation of the beams:

$$w_0(t) = U_0 \sin(\omega_e t) \tag{1}$$

where U_0 is a positive constant and ω_e is the excitation circular frequency.

2.1. Beam equations

The beams are modelled as Euler–Bernoulli beams: i.e. small displacement, small rotation, no transverse shear, and no rotational inertia. The damping of the structure is not considered initially, although it may be introduced easily, either as proportional to the mass and stiffness matrices, or as modal damping. The displacement equation of each beam is

$$m\,\ddot{w}(x,t) + M''(x,t) = -m\,\ddot{w}_0(t) + F_{imp}(t)\delta(x - x_{imp}) \tag{2}$$

where $w(x,t)$ referred to either $w_1(x,t)$ or $w_2(x,t)$, $m = W(\rho_s h_s + \rho_p h_p)$ is the mass per unit length, w is the relative transverse displacement of the beam with respect to the base, and M is the bending moment; F_{imp} is the impact force on the beam located at $x = x_{imp}$ due to the seismic mass (m_s) and the stop (internal wall of the box). The impact is assumed to occur at the tip of the beam ($x_{imp} = L$), except when the impact location influence is addressed. The contact area is assumed to be small compared to the beam dimensions and hence the impact force may be modelled as a concentrated force using the Dirac delta function in (2).

The bending moment may be easily expressed in terms of the transverse displacement as

$$M(x,t) = -W \int_0^h z\, T_1(x,z,t)\, \mathrm{d}z \tag{3}$$

where T_1 is the axial stress in the beam and is related to the strain and the electric field through the following constituent equations:

$$\forall z \in [0\ h_s] \qquad T_1(x,z,t) = Y_s S_1(x,z,t) \tag{4}$$

$$\forall z \in [h_s\ h] \qquad T_1(x,z,t) = \tilde{c}_{11}^E\, S_1(x,z,t) - \tilde{e}_{31} E(x,z,t) \tag{5}$$

with the following definitions.

- E is the electric field, usually supposed to be uniform in a piezoelectric layer, so that

$$E(x,z,t) = E(t)\,\mathbf{1}_{[0,L]}(x)$$

where $\mathbf{1}_{[0,L]}$ is the characteristic function of the interval $[0, L]$. This function could be dropped in this formulation, although it does emphasize the piezoelectric coupling. Note that the local stress at x generates an electric field everywhere between the electrodes. The electric field is derived from the potential $\mathcal{P}$ as

$$E(t) = -\frac{\partial \mathcal{P}}{\partial z}(z,t) \tag{6}$$

and the voltage $v(t)$ between the two electrodes is

$$v(t) = \mathcal{P}(h) - \mathcal{P}(h_s) = -h_p E(t). \tag{7}$$

- S_1 is the axial strain in the beam and considering beam theory one has

$$S_1(x,z,t) = -(z-h_0)\,w''(x,t) \tag{8}$$

where h_0 is the neutral axis position.

As no longitudinal force is applied to the beam, h_0 is defined as

$$W\int_0^h T_1(x,z,t)\,\mathrm{d}x = 0 \tag{9}$$

which leads to

$$h_0 = \frac{Y_s h_s^2 + \tilde{c}_{11}^E (h^2 - h_s^2)}{2(Y_s h_s + \tilde{c}_{11}^E h_p)}. \tag{10}$$

Equations (4)–(8) lead to the following expression for the bending moment:

$$M(x,t) = YI\,w''(x,t) + \mathcal{C}\,h_p\,E(t)\,\mathbf{1}_{[0,L]} \tag{11}$$

with the following definitions.

- YI is the equivalent flexural rigidity of the beam:

$$YI = W\left(Y_s\frac{(h_s-h_0)^3 + h_0^3}{3} + \tilde{c}_{11}^E\frac{(h-h_0)^3 - (h_s-h_0)^3}{3}\right). \tag{12}$$

- $\mathcal{C} = -W\,\tilde{e}_{31}\,h_{pc}$ is an electromechanical coupling factor.
- h_{pc} is the distance between the neutral axis and the mid-layer of the piezoelectric.

Combining (2) and (11) the displacement equation for each piezoelectric beam is

$$\begin{aligned} &m\ddot{w}(x,t) + YIw^{(4)}(x,t) + \mathcal{C}E(t)(\delta'(x) - \delta'(x-L)) \\ &= -m\ddot{w}_0(t) + F_{imp}(t)\delta(x-L). \end{aligned} \tag{13}$$

2.2. Electrical equation

According to the integral form of the Gauss law [11, 21–23], the current i delivered by a pair of electrodes in an admittance circuit (resistor R) is

$$i(t) = \frac{\mathrm{d}Q}{\mathrm{d}t}(t) = \frac{\mathrm{d}}{\mathrm{d}t}\int_A \boldsymbol{D}(x,z,t)\,\mathrm{d}\boldsymbol{A} = \frac{1}{R}v(t) \tag{14}$$

with the following definitions.

- Q is the electric charge on one electrode.
- $\boldsymbol{D}$ is the electric displacement vector. The second piezoelectric constituent relation which holds everywhere in the piezoelectric layer is

$$D_3(x,z,t) = \tilde{e}_{31}\,S_1(x,z,t) + \tilde{\epsilon}_{33}^S E(t). \tag{15}$$

- A is the electrode area.

By substituting (8) and (15) in (14), the electric equation is derived [1, 11, 22, 23]:

$$C_p\,\dot{v}(t) + \frac{1}{R}\,v(t) - \mathcal{C}\int_0^L \dot{w}''(x,t)\,\mathrm{d}x = 0 \tag{16}$$

with the following definitions.

- $C_p = \frac{\tilde{\epsilon}_{33}^S WL}{h_p}$ may be considered as the internal capacitance of the piezoelectric layer.
- $\mathcal{C}$ is the coupling coefficient already found in (11).

Considering the beam boundary conditions, (16) may be rewritten as

$$C_p\,\dot{v}(t) + \frac{1}{R}\,v(t) - \mathcal{C}\,\dot{w}'(L,t) = 0. \tag{17}$$

2.3. Impact model

The impact between two solids has been extensively studied and the phenomena involved in such an event depend on the impact velocity. In the context of impact energy harvesting, low velocity impacts occur giving rise to only local nonlinear deformation and hence the global behaviour is still governed by linear elasticity relationships [15, 16, 24]. The interaction between the seismic mass and each beam is governed by a Hertzian contact law [24–26]. Thus

$$F_{imp}(t) = k_H(w(L,t) - w_m(t))^{(3/2)} \tag{18}$$

where k_H is the Hertzian contact stiffness with nominal value $k_H = 10^7\ \mathrm{N\,m^{-3/2}}$. The interaction force (18) is suitable for the studied device because the end surface of the seismic mass is assumed to be smooth and rounded. The contact stiffness assumes a spherical contact with a radius under 1 μm, and this is discussed further in section 6.1.

This impact model is nonlinear. The nonlinearities arise from the exponent (3/2) in relation (18) and from the contact detection condition. The first nonlinearity implies that the energy stored during the impact depends both on the material characteristics and also on the impact condition (impact velocity). This will be emphasized in section 6.1 and the discussion associated with (43).

2.4. Equations of the whole problem

The piezoelectric problem to be solved is

$$m\ddot{w}^k(x,t) + YI\, w^{k(4)}(x,t) + \mathcal{C}v^k(t)(\delta'(x) - \delta'(x-L)) = -m\ddot{w}_0(t) + F^k_{\text{imp}}(t)\,\delta(x-L) \tag{19}$$

$$C_{\text{p}}\dot{v}^k(t) + \frac{1}{R}v^k(t) - \mathcal{C}\dot{w}'^k(L,t) = 0 \tag{20}$$

for each piezoelectric beam k ($k = 1$ and 2), where $w^k(x,t)$ and $v^k(t)$ are the unknowns.

To complete the problem, the displacement equation of the seismic mass must be added:

$$m_{\text{s}}\,\ddot{w}_{\text{m}}(t) = -F_{\text{imp, beam1}}(t) - F_{\text{imp, beam2}}(t) \tag{21}$$

where $F_{\text{imp,beam}k}(t)$ represents the impact force on beam k due to the seismic mass. A friction force will often occur between the seismic mass and the gliding channel, as remarked by Renaud *et al* [4]; this effect was neglected by Renaud *et al* and is also neglected here.

3. Field displacement discretization

In the following, (19) and (20) are discretized according to a specific Rayleigh–Ritz procedure defined in [17]:

$$w(x,t) = \sum_{i=0}^{\infty} q_i(t)\,\phi_i(x) \tag{22}$$

with the following definitions.

- $\forall\, i > 0$, ϕ_i are the eigenshapes associated with (19) when the piezoelectric layer is in short circuit for a clamped–pinned beam. Thus the beam is subject to an additional boundary condition at the impact location and this system is referred to as the constraint system. ϕ_i is referred to as a constraint shape and the circular eigenfrequencies are denoted ω_i.
- ϕ_{st} is the solution to the static problem of the cantilevered beam where a static force is applied at the impact location ($x = L$) and the displacement at the impact location is equal to unity. Further details about the choice of eigenshapes ϕ_i may be found in [17–19].
- ϕ_0 is the so-called residual mode such as

$$\phi_0(x) = \phi_{\text{st}}(x) - \sum_{i=1}^{\infty} c_i\phi_i(x) \tag{23}$$

  with the coefficients c_i defined so that ϕ_0 is orthogonal to each constraint shape with respect to the mass operator.

The displacement field is better expressed as a function of the parameters $\lambda_i(t) = q_i(t)/c_i$ (with c_0 set equal to unity). Hence

$$w(x,t) = \sum_{0}^{\infty} \lambda_i(t)\, c_i\phi_i(x) \tag{24}$$

$$= \lambda_0\,\phi_{\text{st}}(x) + \sum_{i=1}^{\infty}(\lambda_i(t) - \lambda_0(t))c_i\,\phi_i(x). \tag{25}$$

Note that λ_i does not depend on the normalization of the eigenshapes, $\phi_i(x)$.

The initial distributed model is then discretized by considering only the first $N+1$ terms in the series:

$$w(x,t) = \sum_{i=0}^{N} \lambda_i(t)\, c_i\phi_i(x). \tag{26}$$

4. Discretized equations

4.1. Discretized displacement equations

By substituting expression (26) into (19), the following equation is derived:

$$m\sum_{i=0}^{N}\ddot{\lambda}_i(t)c_i\phi_i(x) + YI\sum_{i=0}^{N}\lambda_i(t)c_i\phi_i^{(4)}(x) - \mathcal{C}v(t)(\delta'(x) - \delta'(x-L)) = -m\ddot{w}_0(x,t) + F_{\text{imp}}(t)\delta(x-L). \tag{27}$$

This is valid for each piezoelectric beam.

The final set of equations is derived by multiplying (27) by $c_j\phi_j(x)$ and then by integrating over the beam length. Two cases have to be considered.

- $j = 0$:

$$m_0\ddot{\lambda}_0(t) + k_0\lambda_0 + \sum_{i=1}^{N} k_i(\lambda_0(t) - \lambda_i(t)) + \mathcal{C}_0 v(t) = -m_{\text{RB},0}\ddot{w}_0(t) + F_{\text{imp}}(t). \tag{28}$$

- $j \neq 0$:

$$m_i\ddot{\lambda}_i(t) + k_i(\lambda_i(t) - \lambda_0(t)) + \mathcal{C}_i v(t) = -m_{\text{RB},i}\ddot{w}_0(t). \tag{29}$$

Here:

- some orthogonal properties proved in [17] are used,
- some properties of the δ distribution are used,
- $\forall\, i > 0$, $m_i = \int_0^L mc_i^2\phi_i(x)^2\,\mathrm{d}x$,
- m_0 is referred to as a residual mass and is the difference between a 'static' mass and the sum of masses $\{m_i\}_{i=1\cdots N}$:

$$m_0 = \int_0^L mc_i^2\phi_{\text{st}}(x)^2\,\mathrm{d}x - \sum_{i=1}^{N} m_i = m_{\text{st}} - \sum_{i=1}^{N} m_i,$$

- $$\forall\, i > 0, \qquad k_i = \int_0^L YIc_i^2\phi_i(x)\,\phi_i^{(4)}(x)\,\mathrm{d}x,$$

- k_0 is the usual static stiffness:

$$k_0 = \int_0^L YI\phi_{\text{st}}(x)\phi_{\text{st}}^{(4)}(x)\,\mathrm{d}x,$$

- $$\mathcal{C}_i = \mathcal{C}c_i\,\phi_i'(L),$$

- $$m_{\text{RB},i} = m\int_0^L c_i\phi_i(x)\,\mathrm{d}x.$$

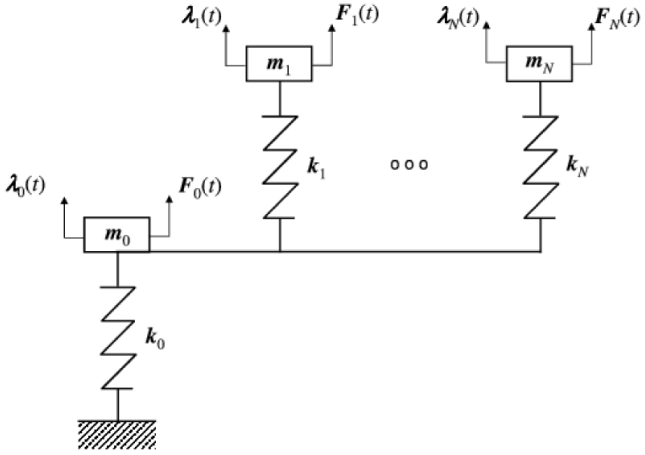

Figure 3. Mechanical model of a piezoelectric cantilevered beam: the piezoelectric coupling is a set of forces included in the forces $F_i(t)$.

These equations may be rewritten as

$$m_0\ddot{\lambda}_0(t) + k_0\lambda_0 + \sum_{i=1}^{N} k_i(\lambda_0(t) - \lambda_i(t)) = F_0(t) \tag{30}$$

$$\forall i > 0, \qquad m_i\,\ddot{\lambda}_i(t) + k_i(\lambda_i(t) - \lambda_0(t)) = F_i(t) \tag{31}$$

where $F_i(t) = -m_{\mathrm{RB},i}\ddot{w}_0(t) - \mathcal{C}_i v(t) + F_{\mathrm{imp}}(t)\delta_{i0}$ (δ_{ij} is the Kronecker delta).

Considering the mechanical aspect of the piezoelectric system, the piezoelectric coupling may be considered as an additional force described by the lumped system shown in figure 3.

Each 1-dof system $\{k_i,\ m_i\}_{i>0}$ is referred to as an anti-oscillator because it may be shown [17] that its natural frequency belongs to the antiresonance frequency set of the studied system. Figure 3 shows that this AO-model extends the 1-dof model of du Toit [9] and may be derived from the AO-model when $N = 0$.

4.2. Discretized electrical equation

By substituting (26) in (20), the discretized electrical equation is

$$C_{\mathrm{p}}\dot{v}(t) + \frac{1}{R}\,v(t) - \sum_{i=0}^{N}\mathcal{C}_i\dot{\lambda}_i(t) = 0. \tag{32}$$

The electric scheme of this equation is a capacitor in parallel with a resistor fed by current sources in parallel. The current delivered by a source is proportional to the velocity.

4.3. Discretized impact model

The definition of eigenshapes ϕ_i and relation (25) infer that $\lambda_0(t)$ has a physical meaning: it represents the transverse displacement at the tip of the beam,

$$\lambda_0(t) = w(L, t). \tag{33}$$

Then equation (18) may be written for each beam as

$$F_{\mathrm{imp}}(t) = k_{\mathrm{H}}(\lambda_0(t) - w_{\mathrm{m}}(t))^{(3/2)}. \tag{34}$$

4.4. Discretized equations of the whole problem

For each piezoelectric beam k, the discretized problem to be solved is

$$m_0\ddot{\lambda}_0^k(t) + k_0\lambda_0^k + \sum_{i=1}^{N} k_i(\lambda_0^k(t) - \lambda_i^k(t)) + \mathcal{C}_0\,v^k(t) = -m_{\mathrm{RB},0}\ddot{w}_0(t) + F_{\mathrm{imp}}^k(t) \tag{35}$$

$\forall i > 0,$

$$m_i\ddot{\lambda}_i^k(t) + k_i(\lambda_i^k(t) - \lambda_0^k(t)) + \mathcal{C}_i\,v^k(t) = -m_{\mathrm{RB},i}\ddot{w}_0(t) \tag{36}$$

$$C_{\mathrm{p}}\dot{v}^k(t) + \frac{1}{R}\,v^k(t) - \sum_{i=0}^{N}\mathcal{C}_i\dot{\lambda}_i^k(t) = 0. \tag{37}$$

The displacement equation of the seismic mass is formally unchanged:

$$m_{\mathrm{s}}\ddot{w}_m(t) = -F_{\mathrm{imp,\,beam1}}(t) - F_{\mathrm{imp,beam2}}(t). \tag{38}$$

When considering an impact problem, a study in the frequency domain is not possible. Indeed, an impact problem is transient by nature and nonlinear: the impact forces depend on the response. Accordingly the problem must be simulated in the time domain. In the following, (35)–(38) are solved by a Newmark-β method for the mechanical variables and a trapezoidal rule for the electrical variables. An implicit Newton–Raphson method is used to deal with the nonlinearities.

The difficulty in solving the problem in the time domain arises from the two different timescales: the high beam natural frequencies and nominal contact stiffness $k_{\mathrm{H}} = 10^7\ \mathrm{N\,m^{-3/2}}$ suggest a sampling time of 10 μs whereas the base movement period is 1 s. In the numerical examples we further discuss the effect of k_{H} on the sample time.

5. Optimization of the piezoelectric device

This section assesses the influence of several design piezoelectric beam parameters (d, gap, L, impact location) on the capability of the studied device to harvest energy. A sensitivity analysis is performed and for several sets of parameters the equations of section 4.4 are solved numerically.

5.1. Nominal case

The material and geometrical characteristics of both beams and the seismic mass are listed in table 1 [3]. The excitation characteristics are given below. The beam's first eigenfrequency in the short-circuit condition is 707 Hz. The equations derived thus far are undamped; a proportional viscous damping could be defined by mass and stiffness matrix proportionality coefficients, as often done in commercial finite element software. However, here it is more appropriate to define the damping using a set of viscous dampers $\{D_i\}$ in parallel with the springs $\{k_i\}$ as

$$D_0 = 2\xi_0\sqrt{k_{\mathrm{st}}m_{\mathrm{st}}} \tag{39}$$

$$D_i = 2\xi_i\sqrt{k_i m_i} \tag{40}$$

Table 1. System characteristics [3].

Beam properties	L (mm)	W (mm)	d (mm)	h_p (μm)	h_s (μm)
	10	5	10	35	105
PZT-5 properties	ϵ_3^S/ϵ_0	$\tilde{e}_{31}$ (F m^{-1})	ρ_p (kg m^{-3})	$\tilde{c}_{11}^E$ (GPa)	
	1500	-10.5	7750	61	
Brass properties	ρ_s (kg m^{-3})	Y (GPa)			
	8500	100			
System properties	m (g m^{-1})	C_p (nF)	$\mathcal{C}$ (μC)	gap (mm)	
	5.8	23.3	-3.03	2.0	

Table 2. Beam excitation [3] and other system parameters.

U_0 (mm)	$T_e = 2\pi/\omega_e$ (s)	m_s (mg)	R (k Ω)
100	1	750	52

Table 3. The AO piezoelectric beam model.

AO number	1	2	3
Mass m_i (mg)	7.1	2.3	1.1
Frequency f_{AO} (kHz)	3.1	10.0	21.0
m_0 (mg)	3.1		
k_{st} (N m^{-1})	278.3		

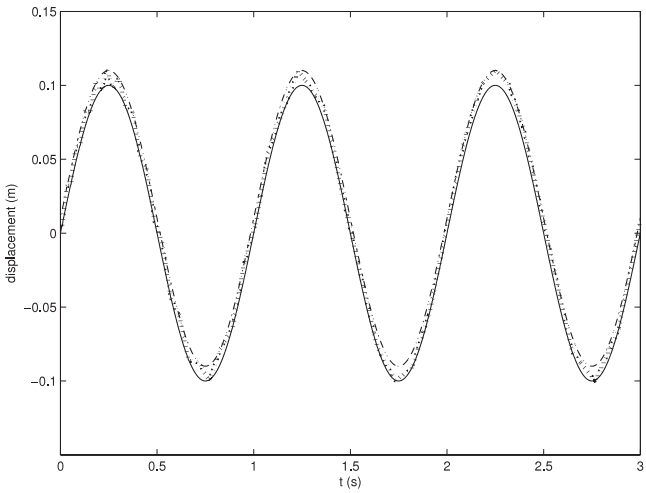

Figure 4. Absolute displacement: beam 1 tip (——), beam 2 tip + d (— · —), seismic mass (· · · · · ·)

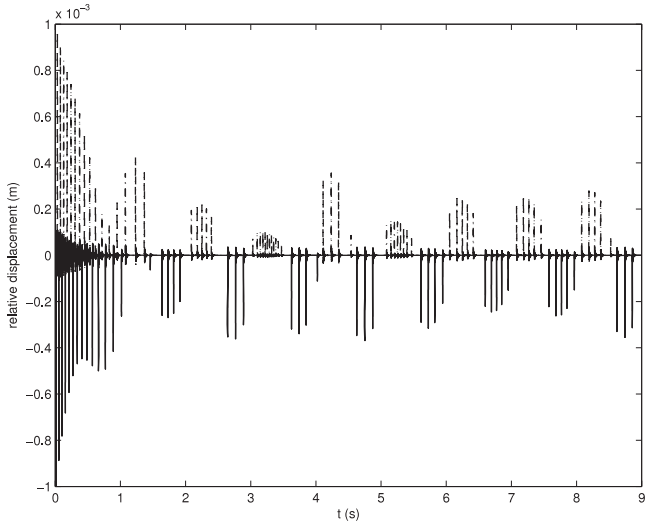

Figure 5. Relative beam tip displacement with respect to the base movement: beam 1 tip (——), beam 2 tip (— · —).

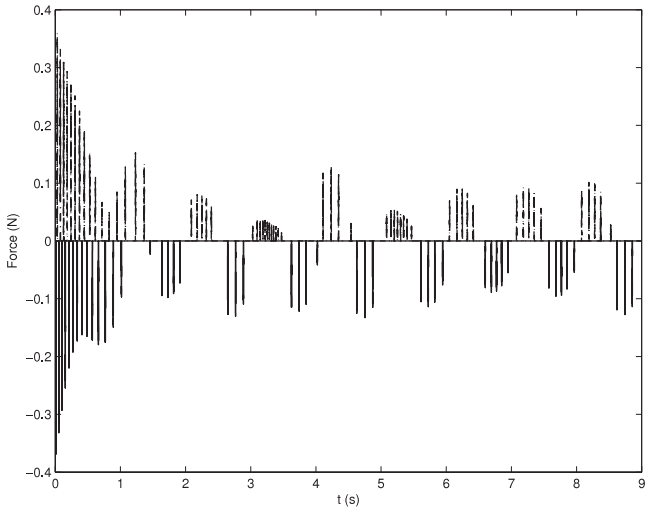

Figure 6. Impact forces on the beams: beam 1 (——), beam 2 (— · —).

where ξ_0 is the piezoelectric beam's first mode damping ratio and ξ_i is the ith mode damping ratio of the piezoelectric beam in the constrained configuration defined in section 4.1. If the damping is well distributed, and if few modes are required, we may assume that all of the damping ratios are equal to ξ_0, which may be experimentally determined. In this paper ξ_0 is set equal to 2.7%, as proposed by Erturk and Inman [1].

The base movement parameters and the seismic mass characteristics are given in table 2. Initially, the seismic mass is placed at the mid-distance between the two beam tips.

The AO-model was derived from a finite element model of the cantilevered beam: each finite element is a Euler–Bernoulli finite element with two dof per node and cubic polynomial interpolation functions. Each beam has been discretized with 20 elements and 3 AOs are considered. The characteristics of the AO-model are given in table 3.

Figures 4–7 show the calculated beam tip displacements (absolute and relative to the root), the impact forces and the voltages obtained from each beam. In figure 4 the beam 2

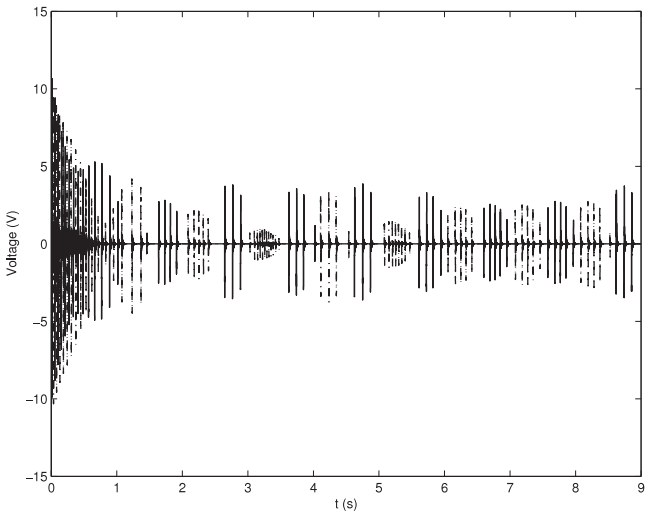

Figure 7. Voltage delivered by each piezoelectric beam: beam 1 (——), beam 2 (— · —).

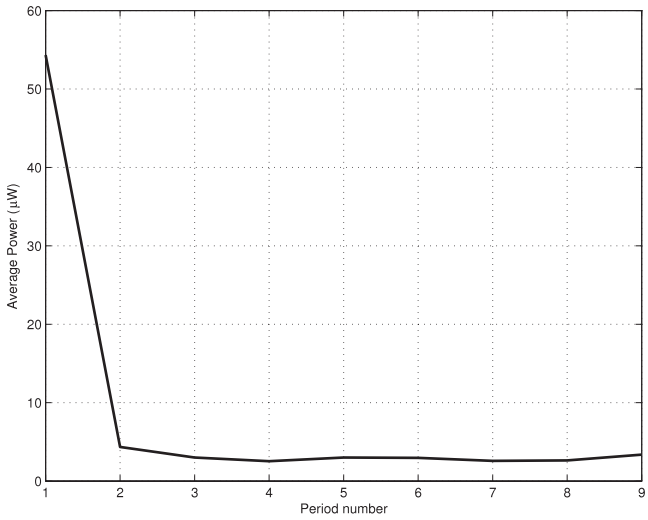

Figure 8. Mean electric power.

displacement is shifted upward by d, the distance between the two beams, so as to represent the limits of the seismic mass displacement. The response has two different behaviours:

- a transient response which lasts mostly during the first base movement period,
- a kind of steady-state response.

This is better illustrated by figure 8, which shows the mean electrical power for the ith cycle of vibration defined as

$$\mathcal{P}(i) = \frac{1}{R} \times \frac{1}{T_e} \int_{i \times T_e}^{(i+1) \times T_e} v^2(t)\, \mathrm{d}t. \tag{41}$$

The mean electric power is almost constant from the second base movement period whereas the power is much greater for the transient movement (first period). Thus we define the transient mean electric power ($\mathcal{P}_{\text{trans}}$) and a steady-state mean electric power ($\mathcal{P}_{\text{steady}}$), which is always much lower than the transient mean electric power. In the following, $\mathcal{P}_{\text{total}}$ is the mean electric power over the whole simulation, and thus lies between $\mathcal{P}_{\text{trans}}$ and $\mathcal{P}_{\text{steady}}$.

The number of dofs has been varied in a convergence study. The results did not change significantly when only one AO was considered, compared to many AOs. This means that each beam is stiff compared to the excitation, and each beam may be modelled as a single-dof system. In the following, only one AO is used, except when mentioned.

5.2. Electric load

To maximize the mean electric power $\mathcal{P}$, the load resistor should be optimized [1, 3]. This resistance is not a mechanical design parameter, but should be optimized for each physical device. For example, as the beam length is varied, the optimum resistor will change. Hence we have to ensure that the optimum resistor is used when we compare the maximum electric power that can be achieved by the studied device.

Several simulations were performed where the load resistance varied from 3 to 300 kΩ. Figure 9 shows the mean power produced for the nominal device parameters, and shows that the maximum mean power is reached for a resistance of 52 kΩ. However there is a plateau between 30 and 200 kΩ where the influence of the resistance is small. The mean power reduces significantly when the system is close to the short-circuit condition (R tends to zero) or close to the open-circuit condition (R tends to infinity). The mean seismic mass kinetic energy was also evaluated and found to be almost constant.

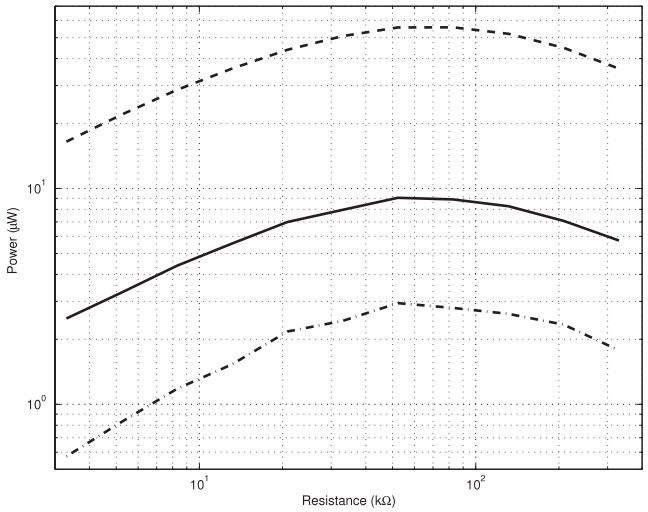

Figure 9. R sensitivity analysis—mean electric power: $\mathcal{P}_{\text{total}}$ (——), $\mathcal{P}_{\text{steady}}$ (— · —), $\mathcal{P}_{\text{trans}}$ (- - - -).

In the following sections, the resistance used is the optimum value for the particular device parameters.

5.3. Optimized mass gliding distance, d

The seismic mass gliding distance has a strong influence on the steady mean electric power as shown in figure 10. Indeed, distance d governs the coupling between the two beams. When d is very small, the coupling is very strong and both beams and the mass move together; accordingly little energy is transferred

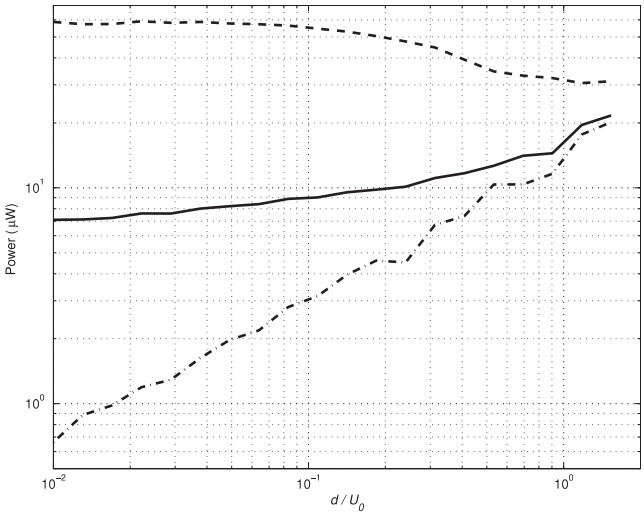

Figure 10. d sensitivity analysis—mean electric power: $\mathcal{P}_{\text{total}}$ (——), $\mathcal{P}_{\text{steady}}$ (— · —), $\mathcal{P}_{\text{trans}}$ (- - - -).

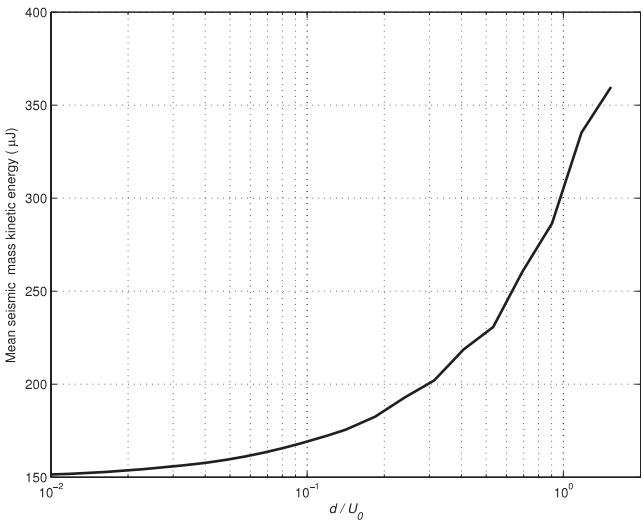

Figure 11. d sensitivity analysis—mean seismic mass kinetic energy.

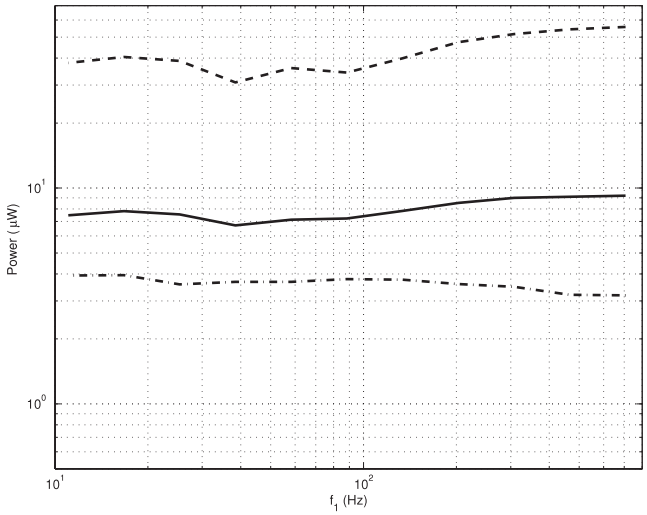

Figure 12. L sensitivity analysis—one AO considered—mean electric power: $\mathcal{P}_{\text{total}}$ (——), $\mathcal{P}_{\text{steady}}$ (— · —), $\mathcal{P}_{\text{trans}}$ (- - - -).

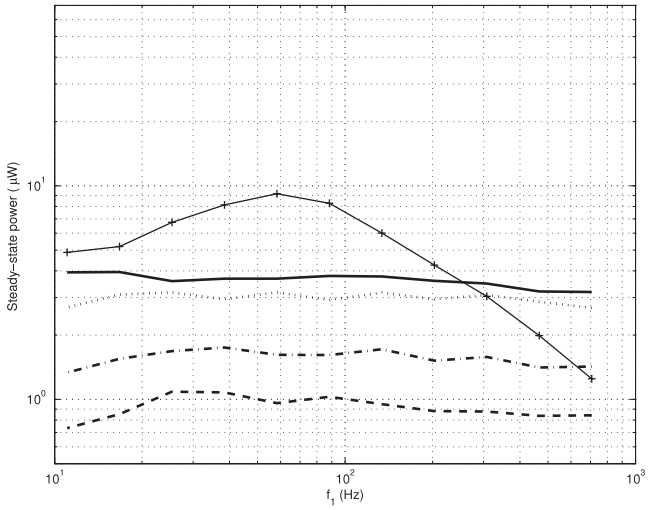

Figure 13. L sensitivity analysis for several load resistors—steady mean electric power: 5 kΩ (– – –), 12 kΩ (— · —), 33 kΩ (· · · · · ·), 52 kΩ (——), 470 kΩ (–+–).

from the mass to the beams because the impact is very smooth. That may be seen in figure 11: the mass kinetic energy increases with d due to a larger relative velocity between the mass and the beams at each impact. The maximum is reached just before d is equal to $2 \times U_0$; at this limit case, the mass does not impact the beams and the power suddenly decreases to that obtained by the base movement only, which is almost zero. Moreover, figure 10 shows that d has little influence on the steady-state mean electric power per unit volume.

No significant influence is detected on the transient electric power.

5.4. Optimized beam length

The beam length has a significant effect on the eigenfrequencies. Increasing the beam length creates a less stiff device. A range of beam lengths has been simulated with the largest length eight times the nominal length, which multiplies the first eigenfrequency by 64. Figure 12 shows that the influence is quite weak. However, the influence of the AO number required to describe the system must be studied to verify whether each beam should be modelled as a single-dof system for greater beam lengths. The simulations showed that three AOs are sufficient to simulate the beam for all lengths and the AO number influence is quite weak. Moreover, the conclusion that the length influence is quite weak still holds even when the first eigenfrequency is lower than 60 Hz (although the effect is noticeable). This means that if the electric power per unit volume is the quantity of interest, a short beam is required.

However the optimized resistance must also be addressed. Indeed, as the dynamics of the system changes, the optimized resistance may change. Figure 13 shows that when the first eigenfrequency is above 300 Hz, 52 kΩ seems to be the optimized resistance, considering the steady-state. However,

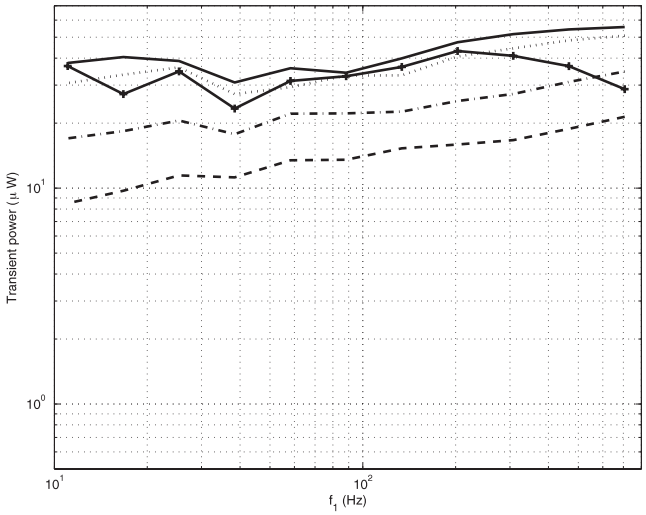

Figure 14. L sensitivity analysis for several load resistors—transient mean electric power: 5 kΩ (– – –), 12 kΩ (— · —), 33 kΩ (· · · · · ·), 52 kΩ (——), 470 kΩ (–+–).

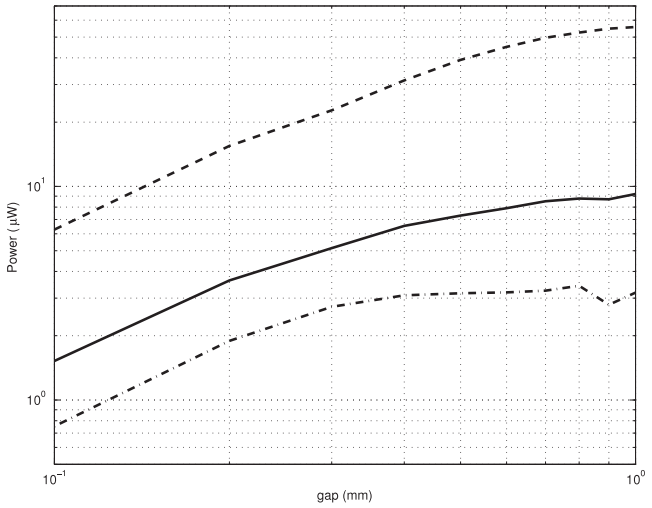

Figure 15. g sensitivity analysis—mean electric power: $\mathcal{P}_{\text{total}}$ (——), $\mathcal{P}_{\text{steady}}$ (— · —), $\mathcal{P}_{\text{trans}}$ (- - - -).

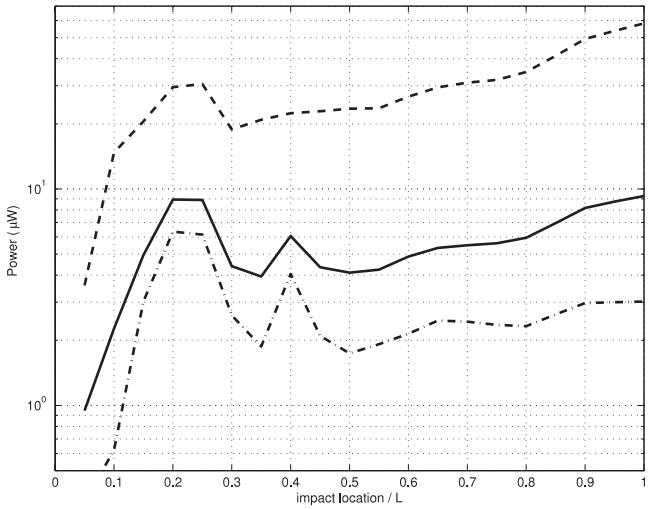

Figure 16. Impact location sensitivity analysis—mean electric power: $\mathcal{P}_{\text{total}}$ (——), $\mathcal{P}_{\text{steady}}$ (— · —), $\mathcal{P}_{\text{trans}}$ (- - - -).

below 300 Hz the optimum resistance may be different and this demonstrates the close connection between the dynamics of a piezoelectric beam and the optimized resistance. For example, for $f_1 = 60$ Hz, $\mathcal{P}_{\text{steady}}$ is three times greater with $R = 470$ kΩ compared to $R = 52$ kΩ. Figure 14 shows that 52 kΩ is an optimized resistance for the transient mean power.

5.5. Optimized gap g

The stop against the wall is unavoidable to have a device volume as small as possible. The stop also limits the beam deformations and keeps the stresses below the failure stress of the piezoelectric material. However, if the gap is too small the beam may be considered as a clamped–pinned beam. As the impact occurs at the pinned end, then no large deformation is produced in the piezoelectric beam and consequently the power generated will be small, as shown in figure 15. Note that the optimum gap is 1 mm as there is no impact against the stop beyond this gap limit.

5.6. Optimized impact location

In a static analysis, for a given force, the maximum deformation energy is reached when the force is applied at the beam tip. However, the situation may be different for a dynamic analysis and hence the impact location was varied from the clamped end to the tip. The stop location is also supposed to vary similarly. Figure 16 shows clearly that $\mathcal{P}_{\text{steady}}$ is optimized if the impact occurs between $0.20 \times L$ and $0.25 \times L$. The optimized resistance varies with the impact location: for example when $x_{\text{imp}} = 0.25 \times L$, R_{opt} is around 10 kΩ. However, it was found that even for a resistance equal to 52 kΩ (i.e. the optimized resistance when $x_{\text{imp}} = L$) the steady-state mean power is greater when $x_{\text{imp}} = 0.25 \times L$ than when $x_{\text{imp}} = L$. This fact is not predictable and is due to the dynamics involved in the impact and the beam response. The large inertial forces from the beam mass close to the beam tip will produce a large deformation in the beam when $x_{\text{imp}} = 0.25 \times L$. The deformation shape becomes more complex and covering the whole beam with piezoelectric material is likely to be a suboptimal solution. Friswell and Adhikari [27] considered different sensor shapes and their analysis may be used to design the optimum coverage of the beam to maximize the energy harvested.

The conclusions are different for $\mathcal{P}_{\text{trans}}$ although it reaches a local maximum in the same range of impact location: its global maximum occurs when the impact is at the beam tip.

5.7. Optimized seismic mass

The harvesting energy device must be as small as possible but should also be as light as possible. Thus we should assess the influence of the seismic mass on the electric power. Figure 17 shows that the mean electric power depends strongly on m_s: the relation between $\mathcal{P}_{\text{steady}}$ and m_s approximates the linear

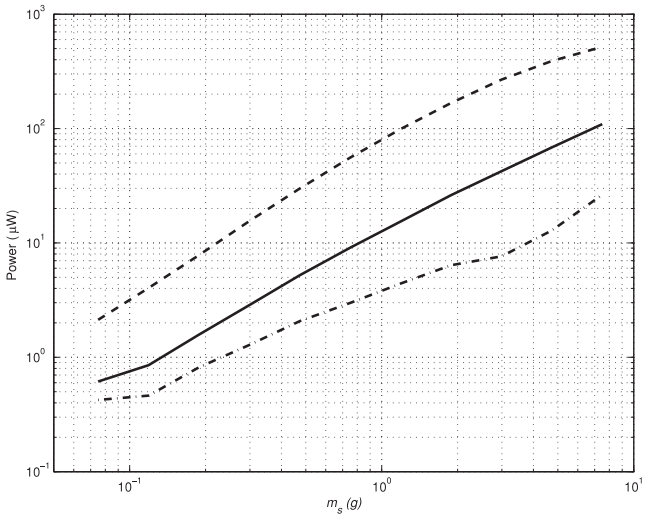

Figure 17. m_s sensitivity analysis—mean electric power: $\mathcal{P}_{\text{total}}$ (——), $\mathcal{P}_{\text{steady}}$ (— · —), $\mathcal{P}_{\text{trans}}$ (- - - -).

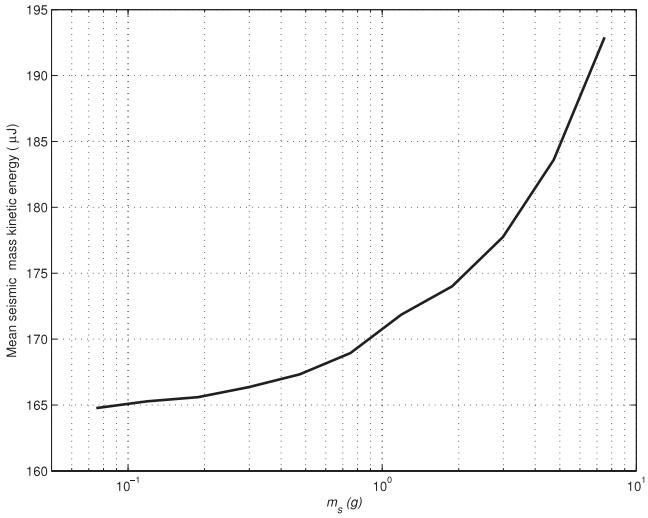

Figure 18. m_s sensitivity analysis—mean seismic mass kinetic energy.

function

$$\tilde{\mathcal{P}}_{\text{steady}} = 3.3 m_s \tag{42}$$

with $\mathcal{P}_{\text{steady}}$ expressed in μW and m_s in g. However, figure 18 shows that the mean seismic mass kinetic energy does not vary so much: an increase by a factor of 100 in the mass only leads to an increase of 17% in the mean kinetic energy. This means that when the mass is increased the seismic mass moves more slowly but produces a higher beam deformation. This is in agreement with the result found by Renaud *et al* [4]. They observed that the ratio of the seismic mass to the effective mass of the beam (constant in this section) has a strong influence on the efficiency of the energy harvester device: a higher ratio (equivalent to a higher seismic mass in our study) produces a higher efficiency.

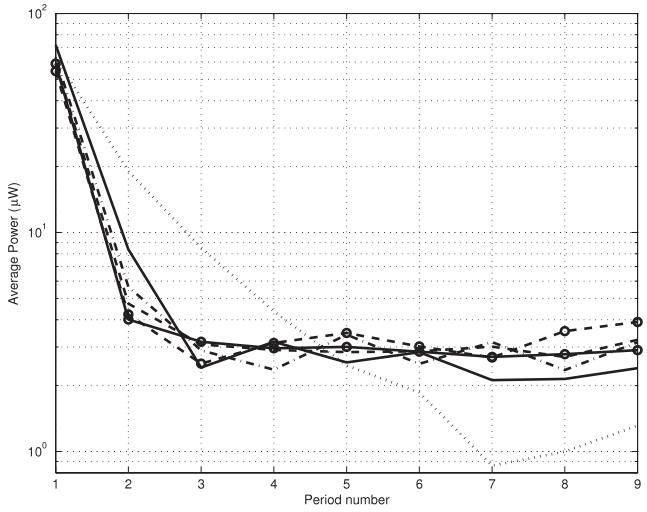

Figure 19. k_{H} sensitivity analysis—mean electric power per base movement period—k_{H} (N m$^{-1.5}$): 10^4 (· · · · · ·), 10^5 (——), 10^6 (— · —), 10^7 (- - o - -), 10^8 (- - - -), 10^9 (—o—).

6. Discussions on damping and contact condition

6.1. Contact condition

As mentioned above, the nominal Hertzian contact stiffness is 10^7 Hz m$^{-1.5}$. This corresponds to a sphere plane contact with the sphere radius lower than 1 μm, which is not very realistic. In this study the sphere radius is around 2 mm, which corresponds to a Hertzian contact stiffness of around 5×10^9 Hz m$^{-1.5}$. The calculations then only converge if the time discretization is less than 1 μs; thus, for a simulation of nine base movement periods, nine million sample points are required and the computational time required for the simulation would increase significantly.

Figure 19 shows that above 10^5 Hz m$^{-1.5}$, k_{H} has almost no influence on the results, and this justifies the Hertzian contact stiffness and the time sampling used in the simulations presented in this paper. Note that all of the curves in figure 19 have been drawn from results obtained with a time discretization equal to 10 μs except the one related to $k_{\text{H}} = 10^9$ Hz m$^{-1.5}$ which was obtained with a time discretization equal to 1 μs.

This k_{H} sensitivity analysis shows that beyond $k_{\text{H}} = 10^5$ Hz m$^{-1.5}$ the contact duration T_{imp} is almost constant (around 5 ms) and produces a similar response of the system. This may be proved by considering the linear stiffness equivalent to the Hertzian contact stiffness [24]

$$k_{\text{lin}} = 0.995(k_{\text{H}}^2\, v_{\text{imp}} \sqrt{m_s})^{2/5}. \tag{43}$$

It turns out that the time duration may be determined as the half-period of an oscillator (m_{eq}, k_{eq}) where k_{eq} is the equivalent stiffness of k_{st} and k_{lin} in series [24, 16, 15]:

$$k_{\text{eq}} = \left(\frac{1}{k_{\text{st}}} + \frac{1}{k_{\text{lin}}} \right)^{-1}. \tag{44}$$

The simulations carried out provided an impact velocity around 0.2 m s^{-1} in the steady-state regime. If $k_{\text{H}} = 10^4$ Hz m$^{-1.5}$

then k_{lin} is close to the static stiffness whereas the ratio k_{lin}/k_{st} is 4.5 (respectively 28.1, 177.3) for $k_H = 10^5$ Hz m$^{-1.5}$ (respectively $k_H = 10^6$ Hz m$^{-1.5}$, $k_H = 10^7$ Hz m$^{-1.5}$). Thus k_{eq} is almost equal to k_{st} when k_H is greater than 10^6 Hz m$^{-1.5}$ and the impact duration, and hence the force spectrum, remains the same. Further details on such studies may be found in [15, 16].

6.2. Dissipation

In an energy harvesting context, mechanical energy dissipation is a quantity that must be minimized to increase the efficiency of the harvester. In a harvesting device many sources of dissipation may occur. For example,

- the internal damping of the structure characterized by the damping ratio ξ;
- the impact dissipation due to the viscoelastic properties of the materials and the transformation into vibrational energy;
- the friction between two solids in contact: this occurs between the seismic mass and the beams as well as the seismic mass and the guiding channel; and
- the dissipation induced by the energy harvesting process.

The friction may be modelled by a Coulomb damping law from the normal force acting on the surfaces in contact. For the beam–projectile contact, no tangential relative movement is supposed to occur and then this dissipation does not happen. However the friction between the mass and the surface of the gliding channel may decrease the performance of the energy harvester: the friction coefficient may be minimized by choosing suitable materials.

The local viscoelastic dissipation has been widely studied and many models have been proposed [26]. In the studied configuration, multiple impacts occur; by introducing the viscous effects, fewer impacts would occur, decreasing the output power. In order to accurately simulate the device, this dissipation must be included in the model. However, this is beyond the scope of this paper and it does not affect the qualitative results obtained in the mechanical optimization study. Note that experimentally Renaud *et al* [4] found a kinematic coefficient of restitution equal to 0.55. In the model developed here, a kinematic coefficient of restitution of 0.87 was found; this coefficient is lower than one due to the conversion of the initial energy into vibrational energy.

As usual in structural dynamics, the internal damping of the beams is modelled by viscous damping. This is the only mechanical dissipation taken into account in this study and is characterized by the damping ratio ξ_0. In practice this damping ratio may be identified easily [28]. Once the materials and the configuration are chosen, it is not possible to optimize this parameter to reduce the loss of energy in structural vibrations. However the damping ratio has a rather small influence on the output power of the energy harvester, as shown in table 4. In this study, to give a conservative estimate of the harvested energy a relatively large damping ratio was used, as proposed by Erturk and Inman [1]. Renaud *et al* [4] proposed a mechanical quality factor Q of 50, which is equivalent to a damping ratio $\xi = 1/(2Q)$, or 1%. The simulations have shown that when this lower value is used, higher output powers are obtained but the conclusions about the mechanical optimization are the same.

Table 4. Output power for several damping ratios.

ξ_0 (%)	$\mathcal{P}_{trans}$ (μW)	$\mathcal{P}_{steady}$ (μW)
5.0	47.0	2.7
2.7	54.4	2.9
1.0	65.0	3.4

Lesieutre *et al* [29] investigated the damping that results from the piezoelectric energy harvesting process. They also showed that the influence of a nonlinear electronic interface required to convert and store the electric energy is strong. Lefeuvre *et al* [30] studied several electrical interfaces to improve the efficiency of the electromechanical conversion. However, the optimization of the electrical design parameters is outside the scope of this paper.

Dissipation modelling is a difficult task in structural dynamics and, if possible, must be minimized. However it has only a small influence on the harvesting problem and does not influence the conclusions obtained in section 5.

7. Comments and conclusion

A new model for piezoelectric beams has been presented in this paper which leads to a lumped model where the piezoelectric effect is described through the applied forces. This model is especially appropriate to solve impact problems.

A piezoelectric device for impact energy harvesting has been simulated and two regimes have been identified that may be described as transient and steady-state. This result is predictable for harmonic base excitation. However, the presence of the impacts means that the steady-state response cannot be obtained directly in the frequency domain.

Sensitivity analysis has been performed with respect to several design parameters to optimize the device. The device performance has been quantified by two quantities: the transient mean electric power $\mathcal{P}_{trans}$ and the steady-state mean electric power $\mathcal{P}_{steady}$, which is much lower than $\mathcal{P}_{trans}$. As the base movement is harmonic, $\mathcal{P}_{steady}$ is the most relevant quantity to characterize the device. However, $\mathcal{P}_{trans}$ represents the maximum mean electric power that could be obtained if the transient regime persisted.

The sensitivity analysis has shown that an optimal load resistor may be determined. However, if the electric load is far from the limit cases (short circuit and open circuit), the electric load only has a weak influence on the device performance. It has also been shown that the optimal electric load may vary significantly with the piezoelectric beam stiffness. The stop gap is mainly required for safety, and this gap should be as large as possible providing the maximum beam stress is not above the elastic yield stress.

The width of the device, which is closely related to the seismic mass gliding distance, d, should be chosen based on the base movement amplitude U_0: the best performance is achieved when d is just lower than two times U_0. However, a compromise is required between the output electric power and

the device width. The length, that is the piezoelectric beam stiffness, has no significant influence on the performance.

As the output electric power was found to vary linearly with the seismic mass, the optimal weight of the device is a compromise between the weight and the performance.

The impact location turned out to be a significant parameter that does not affect the device volume. The maximum electric power is not obtained when the impact is located at the beam tip.

Acknowledgments

The first author acknowledges the financial support from University of Lyon for his six-month academic sabbatical leave. This research was performed at Swansea University.

References

[1] Erturk A and Inman D J 2009 An experimentally validated bimorph cantilever model for piezoelectric energy harvesting from base excitations *Smart Mater. Struct.* **18** 025009
[2] Adhikari S, Friswell M I and Inman D J 2009 Piezoelectric energy harvesting from broadband random vibrations *Smart Mater. Struct.* **18** 115005
[3] Renaud M, Fiorini P and Van Hoof C 2007 Optimization of a piezoelectric unimorph for shock and impact energy harvesting *Smart Mater. Struct.* **16** 1125–35
[4] Renaud M, Fiorini P, van Schaijk R and Van Hoof C 2009 Harvesting energy from the motion of human limbs: the design and analysis of an impact-based piezoelectric generator *Smart Mater. Struct.* **18** 0035001
[5] Moss S, Barry A, Powlesland I, Galea S and Carman G P 2010 A low profile vibro-impacting energy harvester with symmetrical stops *Appl. Phys. Lett.* **97** 234101
[6] Smits J and Choi W-S 1991 The constituent equations of piezoelectric heterogeneous bimorphs *IEEE Trans. Ultrason. Ferroelectr. Freq. Control* **38** 256–70
[7] Wang Q-M and Cross L E 1999 Constitutive equations of symmetrical triple layer piezoelectric benders *IEEE Trans. Ultrason. Ferroelectr. Freq. Control* **46** 1343–51
[8] Ballas R G, Schlaak H F and Schmid A J 2006 The constituent equations of piezoelectric multilayer bending actuators in closed analytical form and experimental results *Sensors Actuators* A **130/131** 91–8
[9] du Toit N E, Wardle B L and Kim S-G 2005 Design considerations for mems-scale piezoelectric mechanical vibration energy harvesters *Integr. Ferroelectr.* **71** 121–60
[10] Erturk A and Inman D J 2008 Issues in mathematical modeling of piezoelectric energy harvesters *Smart Mater. Struct.* **17** 065016
[11] Erturk A and Inman D J 2008 A distributed parameter electromechanical model for cantilevered piezoelectric energy harvesters *J. Vib. Acoust.* **130** 041002
[12] Sodano H A, Park G and Inman D J 2004 Estimation of electric charge output for piezoelectric energy harvesting *J. Strain* **40** 49–58
[13] Ries L L and Smith W 1999 Finite element analysis of a deformable array transducer *IEEE Trans. Ultrason. Ferroelectr. Freq. Control* **46** 1352–63
[14] De Marqui C Junior, Erturk A and Inman D J 2009 An electromechanical finite element model for piezoelectric energy harvester plates *J. Sound Vib.* **327** 9–25
[15] Pashah S, Massenzio M and Jacquelin E 2008 Prediction of structural response for low velocity impact *Int. J. Impact Eng.* **35** 119–32
[16] Pashah S, Massenzio M and Jacquelin E 2008 Structural response of impacted structure described through anti-oscillators *Int. J. Impact Eng.* **35** 471–86
[17] Jacquelin E, Lainé J P, Bennani A and Massenzio M 2007 A modelling of an impacted structure based on constraint modes *J. Sound Vib.* **301** 789–802
[18] Jacquelin E, Lainé J P, Bennani A and Massenzio M 2008 The anti-oscillator model parameters linked to the apparent mass frequency response function *J. Sound Vib.* **312** 630–43
[19] Jacquelin E, Lainé J P and Massenzio M 2009 The antioscillator model and the finite element method *J. Sound Vib.* **324** 317–31
[20] Jacquelin E 2009 On the rigid projectile model for low velocity impacts *Int. J. Impact Eng.* **36** 1006–11
[21] *IEEE Standard on Piezoelectricity* 1987 (Piscataway, NJ: IEEE)
[22] Weinberg M S 1999 Working equations for piezoelectric actuators and sensors *J. Electromech. Syst.* **8** 529–33
[23] Lu F, Lee H P and Lim S P 2004 Modeling and analysis of micro piezoelectric power generators for micro-electromechanical-systems applications *Smart Mater. Struct.* **13** 57–63
[24] Stronge W J 2000 *Impact Mechanics* (Cambridge: Cambridge University press)
[25] Abrate S 1998 *Impact on Composite Structures* (Cambridge: Cambridge University Press)
[26] Acary V and Brogliato B 2004 Coefficients de restitution et efforts aux impacts. Revue et comparaison des estimations analytiques *Technical report* INRIA
[27] Friswell M I and Adhikari S 2010 Sensor shape design for piezoelectric cantilever beams to harvest vibration energy *J. Appl. Phys.* **108** 014901
[28] Ewins D J 2000 *Modal Testing: Theory and Practice* 2nd edn (Baldock: Research Studies Press)
[29] Lesieutre G A, Ottman G K and Hofmann H F 2004 Damping as a result of piezoelectric energy harvesting *J. Sound Vib.* **269** 991–1001
[30] Lefeuvre E, BAdel A, Richard C, Petit L and Guyomar D 2006 A comparison between several vibration-powered piezoelectric generators for standalone systems *Sensors Actuators* A **126** 405–16